Staggered Multiple-PRF Ultrafast Color Doppler

Daniel Posada, Jonathan Porée, Arnaud Pellissier, Boris Chayer, François Tournoux, Guy Cloutier, and Damien Garcia*

Abstract—Color Doppler imaging is an established pulsed ultrasound technique to visualize blood flow non-invasively. High-frame-rate (ultrafast) color Doppler, by emissions of plane or circular wavefronts, allows severalfold increase in frame rates. Conventional and ultrafast color Doppler are both limited by the range-velocity dilemma, which may result in velocity folding (aliasing) for large depths and/or large velocities. We investigated multiple pulse-repetition-frequency (PRF) emissions arranged in a series of staggered intervals to remove aliasing in ultrafast color Doppler. Staggered PRF is an emission process where time delays between successive pulse transmissions change in an alternating way. We tested staggered dual- and triple-PRF ultrafast color Doppler, 1) *in vitro* in a spinning disc and a free jet flow, and 2) *in vivo* in a human left ventricle. The *in vitro* results showed that the Nyquist velocity could be extended to up to 6 times the conventional limit. We found coefficients of determination $r^2 \geq 0.98$ between the de-aliased and ground-truth velocities. Consistent de-aliased Doppler images were also obtained in the human left heart. Our results demonstrate that staggered multiple-PRF ultrafast color Doppler is efficient for high-velocity high-frame-rate blood flow imaging. This is particularly relevant for new developments in ultrasound imaging relying on accurate velocity measurements.

Index Terms—De-aliasing, Nyquist velocity extension, staggered multiple-PRF, ultrafast color Doppler.

I. INTRODUCTION

COLOR Doppler ultrasound is the most widespread clinical imaging modality to analyze blood circulation. It maps the blood flow, non-invasively and in real time, by transmitting uniformly delayed ultrasound pulses from which received echoes are processed to determine velocities. Even if two-dimensional color Doppler has extensive clinical applications, it is still used mainly for qualitative mapping of flow properties. Typical echocardiographic applications include, *e.g.*, visualization of valvular regurgitations, detection of septal defects, or guiding the positioning of the pulsed-wave sample volume for spectral flow analysis. Recent innovative tools have been introduced to make color Doppler more quantitative. For example, it can better decipher the intracardiac flow dynamics by using vector flow mapping (vector flow mapping enables reconstruction of 2-D flow velocity fields in cardiac cavities) [1], [2] or Doppler vortography that can assess blood flow vortices in heart chambers [3]. These tools are potentially relevant since the dynamics of the main intraventricular vortex is related to the cardiac function [4], [5]. Quantitative velocity maps may thus help clinicians make headway in cardiac diagnosis. The challenge is however important as intracardiac flow is highly non-stationary and contains high velocities. Although high-velocity high-frame-rate Doppler imaging is needed for cardiac flow quantification, cardiac color Doppler is currently limited by low frame rates and aliased (wrapped) velocities. The objective of this *in vitro* and *in vivo* study was to propose staggered multiple-PRF high-frame-rate color Doppler to get time-resolved alias-free Doppler velocity fields.

A. High Frame Rates in Color Doppler

To get a time-resolved flow analysis of transient events, current methods rely on successive cardiac cycles that must be temporally registered to compensate for the low frame rates of clinical Doppler scanners (typically $\sim$ 10 frames per second, FPS, for cardiac applications). Conventional color Doppler reaches such limited temporal resolutions because several series of focused beams are needed to generate one image. Conversely, emissions of wide wavefronts can override the frame rate limitation and broaden the clinical perspectives of blood flow ultrasound imaging [6], [7]. Accurate vector flow imaging in carotid arteries is one of the promising potentials of plane wave color Doppler [8], [9]. Diverging beams have also been proposed to exploit the benefits of ultrafast ultrasound in ultrasound Doppler imaging [10], [11]. Recently, ultrafast color Doppler was extended to 3-D in vascular and cardiac flow imaging [12]. It is likely that ultrafast color Doppler may supplant conventional color Doppler in the near future. The possibility to increase the frame rate several folds indeed offers new opportunities in flow imaging.

B. Alias-Free Color Doppler

No matter the scanning mode (conventional or ultrafast), another limitation for quantitative color Doppler techniques is

the presence of aliasing (*i.e.*, velocity folding). Aliasing occurs when the flow information is time-sampled insufficiently. As Doppler velocity exceeds a certain magnitude, it is aliased (wrapped around) to the opposite side of the Doppler spectrum [13]. In the classical red-blue Doppler color map, aliased velocities turn from red to blue or *vice versa*, potentially creating ambiguity in interpretation. Recovering true velocities in color Doppler ultrasound is an essential condition for quantitative blood flow analysis. Dealiasing (or unwrapping) is the process of recovering the actual velocities (or phases) from the wrapped velocities (or phases). The most advanced unwrapping approaches were most likely developed in the family of imaging based on interferometry, principally InSAR (interferometric synthetic aperture radar) [14]. A few techniques have also been proposed to dealias Doppler blood velocities by image post-processing of pre or post scan-converted color Doppler images [15], [16]. Unwrapping or dealiasing is an ill-posed problem if no additional information is given. Most unwrapping algorithms thus assume that the actual velocities (or phases) of connected pixels are close enough to avoid discontinuity after unwrapping (as in [15]). More complex algorithms and *a priori* knowledge may be required if the true velocity map is discontinuous or if the aliased data are noisy. These unwrapping techniques are relatively compute-intensive and cannot be considered for real-time visualization of alias-free color Doppler.

C. Multiple-PRF Color Doppler

In our study, in contrast to the abovementioned post-processing approaches, we took advantage of the high frame rate of ultrafast ultrasound to extend the Nyquist limit of color Doppler by using a specific transmission strategy. To this end, we employed multiple-PRF staggered schemes inspired from weather radar [17] to disambiguate the Doppler fields. Staggered PRF is an emission process where time delays between successive pulses change in an alternating way [18]. For example, if the PRP_i denote the pulse repetition periods, a dual-staggered PRF system emits at instants $t_0, t_0 + PRP_1, t_0 + PRP_1 + PRP_2, \dots, t_0 + nPRP_1 + (n-1)PRP_2, t_0 + nPRP_1 + nPRP_2, \dots$ (Fig. 1). In such a dual-PRF sequence, the autocorrelations at lag PRP_1 and at lag PRP_2 can be combined to estimate Doppler velocities from the difference of the two phases (see (7) in [19]). It follows that the maximal speed that can be estimated is determined by the absolute difference $|PRP_1 - PRP_2|$ [18]. In words, a multiple-PRF system behaves as if the pulse repetition frequency has been synthetically increased, thus extending the Nyquist velocity limit. Dual-PRF approaches were originally proposed in the 70's to solve the aliasing problem in Doppler weather radar. Emission of different suitably combined pulses can indeed lead to a severalfold increase in the actual Nyquist velocity [20]. Nishiyama *et al.* and Nogueira proposed the use of staggered dual-PRF sequences to extend the non-ambiguous velocity interval in pulsed Doppler [21], [22]. Their methods were similar to that proposed in the weather radar literature. With this technique, autocorrelation estimates are combined to obtain the velocity from the phase difference of the two pulse series [19]. Nitzpon *et al.* used another tactic and described a system equipped with a transmitter capable of generating pulses
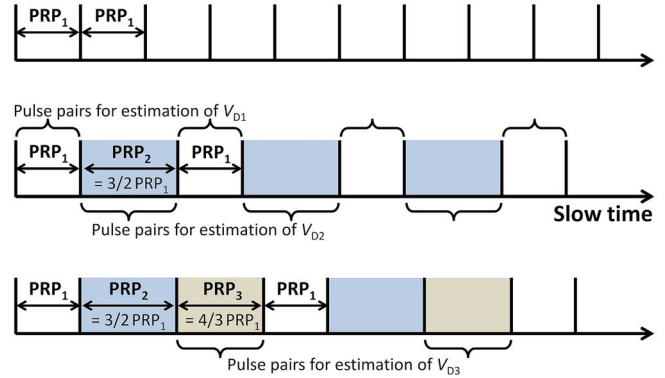

Fig. 1. Staggered multiple-PRF sequences. The top sequence represents the conventional equally-spaced transmission strategy (PRP = pulse repetition period). The respective 2nd and 3rd sequences represent dual- and triple-PRF schemes; pairs of pulses are emitted with delays changing sequentially. These pulse pairs are used to generate several Doppler images (V_{D_i}), which are combined to disambiguate the Doppler velocity field.

with two different carrier frequencies. This system produced two velocity estimates sequentially that were joined to measure blood velocities beyond the Nyquist limit [23].

In this study, by using dual- or triple-PRF strategies (Fig. 1) in ultrafast ultrasound imaging, we were able to extend the Nyquist velocity several folds to produce non-aliased Doppler images, both *in vitro* and *in vivo*. For this purpose, we developed an original and simple fast numerical method which recovers the Nyquist numbers. The Nyquist number is the integer that represents the number of Nyquist intervals the true velocity deviates from the measured value [24]. In the following, we first describe our staggered multiple-PRF method and dealiasing procedure. We next present *in vitro* results obtained in a spinning disk and in a free jet flow. We finally illustrate the efficacy of our approach using *in vivo* ultrafast Doppler data acquired in a human left heart.

II. METHODS

Dual-PRF pulsing strategy is nowadays implemented in many types of meteorological radars. In this paper, we propose a multiple-PRF strategy, *i.e.* the number of different PRFs is not limited to two. In this section, we describe this multiple-PRF approach and explain how additional PRFs must be chosen. We also put forward an original dealiasing procedure based on the estimation of Nyquist numbers and provide a thorough theoretical description. This technique was tested *in vitro* and *in vivo* with 2 or 3 staggered PRFs. The proposed method simply results in a lookup table, which facilitates implementation and accelerates processing.

A. Theoretical Background—Staggering the PRF to Extend the Nyquist Velocity

In both conventional and ultrafast color Doppler imaging, a series of pulses is transmitted at a given rate to estimate the velocity of moving scatterers (see first row in Fig. 1). According to the Nyquist-Shannon sampling theorem, there is a maximum speed that can be determined without ambiguity. This speed limit is referred to as the Nyquist velocity (V_N) [25]:

$$V_N = \frac{PRF\lambda}{4}, \tag{1}$$

where PRF (pulse repetition frequency) is the number of ultrasound transmissions per second (*i.e.* the slow-time sampling frequency), and λ is the wavelength associated to the transducer central frequency. Aliasing occurs when absolute Doppler velocities higher than the Nyquist velocity (1) are folded back into the Nyquist interval. The time lag between two consecutive pulses (pulse repetition period, $\mathrm{PRP} = 1/\mathrm{PRF}$) also limits the maximum depth that can be imaged, since the PRP must be long enough to allow back-and-forth traveling of transmitted echoes. The color Doppler trade-off between the maximum range depth ($r_{\max}$) and the maximum velocity can be expressed by the following range-velocity product [25]:

$$r_{\max} V_{\mathrm{N}} = \frac{c\lambda}{8}, \tag{2}$$

where c is the speed of sound (~ 1540 m/s in soft tissues). For a given wavelength, (2) illustrates that it is generally impossible to measure high flow velocities without ambiguity in deep tissues. For example, using a 2.5 MHz cardiac phased-array and a maximum range of 20 cm (as with an apical long axis view in an adult), a maximum speed of only 0.6 m/s can be measured. Typical mitral E-wave velocities are ~ 0.8 m/s and can be > 1 m/s in patients with restrictive filling [26]. Aliasing is therefore prevalent in Doppler echocardiography, even in the absence of valvular disease. A multiple-PRF approach can help to obtain unaliased color Doppler, as explained in what follows.

The unambiguous (*i.e.* alias-free) Doppler velocity (V_{D}^{u}) is related to the measured Doppler velocity (V_{D}) by [27]:

$$V_{\mathrm{D}} = V_{\mathrm{D}}^{u} - 2n_{\mathrm{N}}V_{\mathrm{N}}, \tag{3}$$

where n_{N} is the Nyquist number (with $n_{\mathrm{N}} \in \mathbb{Z}$). Doppler velocities are aliased when $n_{\mathrm{N}} \neq 0$. The Nyquist number can be expressed as (see the demonstration in Appendix):

$$n_{\mathrm{N}} = \mathrm{floor}\left(\frac{V_{\mathrm{D}}^{u} + V_{\mathrm{N}}}{2V_{\mathrm{N}}}\right), \tag{4}$$

where $\mathrm{floor}(x)$ is the largest integer less than or equal to x. It is noticeable that Doppler velocities can be dealiased from (3) if the corresponding Nyquist integers are known; however, this is not the case in general. Staggering two or more pulse repetition frequencies can help to determine the Nyquist numbers to some extent. The idea is to produce several specific sequences (2 or 3 in our study), each of different period, that alias differently. Using such sequences, the Nyquist numbers can be estimated from the velocity differences, as described in this subsection.

Fig. 1 illustrates three different pulsing sequences: the conventional equally spaced pulsing sequence, as well as staggered PRF sequences in which pulses are interlaced using two or three different PRFs. Sirmans *et al.* described how the staggered PRF mode can be used to broaden the unambiguous velocity interval [18]. Their method determines two Doppler velocities V_1 and V_2, the first one from paired pulses delayed by PRP_1 (pulse repetition period #1), and the second one from paired pulses delayed by PRP_2 (pulse repetition period #2). To extend the unambiguous velocity range, one of the Doppler estimates is adjusted by an amount dictated by the Doppler velocity difference ($V_2 - V_1$). We developed a derived approach and generalized this concept by seeking the Nyquist numbers. We here give an in-depth theoretical analysis and describe how the supplementary PRFs must be selected.

Let PRF_1 (pulse repetition frequency #1) correspond to the greater PRF. Neglecting the duty cycle, a typical value for PRF_1 can be selected according to the maximal range depth to avoid overlaid echoes:

$$\mathrm{PRF}_1 = \frac{c}{2r_{\max}} \tag{5}$$

whose corresponding Nyquist velocity is deduced from (1):

$$V_{\mathrm{N}_1} = \frac{\mathrm{PRF}_1\lambda}{4}. \tag{6}$$

A multiple-PRF pulse sequence can extend the Nyquist velocity given by (6). Although we used a dual- or triple-PRF strategy in this study, as illustrated in Fig. 1, the following description remains valid for any number of interleaved PRFs. Before getting through the proposed dealiasing process, let us first describe the multiple-PRF sequences. In addition to the main pulse repetition frequency PRF_1, supplementary smaller PRFs (*i.e,* $\mathrm{PRF}_i < \mathrm{PRF}_1$, for $i > 1$) are implemented to make the full emission sequence staggered (Fig. 1). Note that the additional PRF_i must be smaller to prevent competing echoes. As will become clear shortly, it is convenient to express the PRF in terms of ratio of relatively prime positive integers:

$$\mathrm{PRF}_i = \frac{p_i}{q_i}\mathrm{PRF}_1, \tag{7}$$

with p_i and q_i positive integers such that $p_i = q_i = 1$ if $i = 1$, and $p_i < q_i$ and $(p_i, q_i) = 1$ (*i.e,* p_i and q_i are relatively prime) otherwise. This implies (from (1)):

$$V_{\mathrm{N}_i} = \frac{p_i}{q_i}V_{\mathrm{N}_1}. \tag{8}$$

From these individual Nyquist velocities, the extended Nyquist velocity (V_{N_e}) of the multiple-PRF scheme can be deduced. The extended Nyquist velocity is the smallest velocity that verifies $V_{\mathrm{N}_e} = n_i V_{\mathrm{N}_i}$, $\forall i \geq 1$, where n_i is a positive integer [28]. According to (8), the extended Nyquist velocity is thus given by [28]:

$$V_{\mathrm{N}_e} = \mathrm{LCM}(p_2, \ldots, p_i, \ldots)V_{\mathrm{N}_1} \equiv kV_{\mathrm{N}_1}, \tag{9}$$

where LCM denotes the least common multiple. As an illustration of what would happen in a particular case of a triple-PRF scheme, let $\mathrm{PRF}_2 = 2/3\ \mathrm{PRF}_1$ and $\mathrm{PRF}_3 = 3/4\ \mathrm{PRF}_1$. This sequence provides a six-fold increase in the Nyquist velocity since (9) gives $V_{\mathrm{N}_e} = \mathrm{LCM}(2, 3)V_{\mathrm{N}_1} = 6V_{\mathrm{N}_1}$. More generally, (9) shows that the larger the integers p_i (and thus the nearer the additional PRF_i are to PRF_1), the larger is the extended Nyquist velocity. In practice, however, they cannot be too large, as explained later.

We know from (9) that a multiple-PRF sequence can theoretically increase the Nyquist velocity up to V_{N_e}. We now need a simple process to unwrap the aliased Doppler velocities given by this specific radiating sequence. This can be achieved by calculating the Nyquist numbers. A multiple-PRF scheme gives rise to several Doppler velocities (V_{D_i}), which all verify (3):

$$V_{\mathrm{D}}^{u} = V_{\mathrm{D}_i} + 2n_{\mathrm{N}_i}V_{\mathrm{N}_i}, \tag{10}$$

where n_{N_i} and V_{N_i} are the corresponding Nyquist number and Nyquist velocity. To mitigate the effects of velocity ambiguities, we need to obtain the Nyquist numbers n_{N_i}. This is possible (in some range reported below) because the n_{N_i} are integers. Let us first determine the ranges of the Nyquist numbers for which the Doppler velocity field can be fully dealiased. The unambiguous Doppler velocities can be resolved whenever their absolute values are less than the extended Nyquist velocity $V_{N_e} = k V_{N_1}$ (with $k = \text{LCM}(p_2, \ldots, p_i, \ldots)$, see (9)):

$$|V_D^u| < k V_{N_1}. \tag{11}$$

Applying (4), it can be shown that this remains true if the Nyquist numbers are bounded by (see the demonstration in Appendix):

$$|n_{N_i}| \leq \text{ceiling}\left(\frac{k q_i}{2 p_i} - \frac{1}{2}\right), \tag{12}$$

where ceiling(x) gives the smallest integer greater than or equal to x. To disambiguate the Doppler velocity field, we can now determine the Nyquist numbers n_{N_i} present in (10). Combining (8) and (10) gives:

$$q_i \frac{V_{D_i} - V_{D_1}}{2 V_{N_1}} = n_{N_1} q_i - n_{N_i} p_i. \tag{13}$$

The right-hand side in (13) is an integer. But, in practice, the left-hand side is not an integer due to observational errors in the measured Doppler velocities (V_{D_i} and V_{D_1}). Equation (13) is thus rewritten as:

$$\text{nint}\left(q_i \frac{V_{D_i} - V_{D_1}}{2 V_{N_1}}\right) = n_{N_1} q_i - n_{N_i} p_i, \tag{14}$$

where nint() denotes the nearest integer. In a multiple-PRF design with N_{PRF} PRFs related by (7) (where $N_{PRF} = 2$ or 3, for a dual- or triple-PRF sequence, respectively), (14) leads to an undetermined system with N_{PRF} unknowns (i.e., the Nyquist numbers, n_{N_i}) and $(N_{PRF} - 1)$ independent equations. One could think that system (14) cannot be solved at first glance. Let us recall, however, that the Nyquist numbers are integers. Furthermore, they are constrained by inequality (12). This guarantees the uniqueness of the solution in the ranges defined by (12). As a side note, another constraint can be derived to condense the lookup table proposed below. This second constraint limiting the ranges of the Nyquist numbers is given by (see the demonstration in Appendix):

$$|n_{N_1} q_i - n_{N_i} p_i| \leq \frac{1}{2}(p_i + q_i). \tag{15}$$

To understand how (12), (14) and (15) can be used to determine the Nyquist numbers, let us illustrate a dual-PRF scheme with $PRF_2 = 3/4 \, PRF_1$, *i.e*, $p_2 = 3$ and $q_2 = 4$. According to the expression of the extended Nyquist velocity in (9), we have $k = 3$. In this particular case, the extended Nyquist velocity is thus three-fold the original Nyquist velocity (*i.e.*, $V_{N_e} = 3 V_{N_1}$). The inequality (12) yields the ranges for the Nyquist numbers that ensure full unwrapping, which are in this example: $|n_{N_1}| \leq 1$ and $|n_{N_2}| \leq 2$. Using these bounds, the different value combinations given by (14) are given in the lookup Table I. Note that the additional constraint (15) has been applied

$\text{nint}\left(q_2 \dfrac{V_{D_2} - V_{D_1}}{2 V_{N_1}}\right)$	n_{N_1}	n_{N_2}
-3	0	1
-2	1	2
-1	-1	-1
0	0	0
1	1	1
2	-1	-2
3	0	-1

to optimize this table and limit the solution to 7 possible combinations. A triple-PRF scheme with $PRF_2 = 2/3 \, PRF_1$ and $PRF_3 = 3/4 \, PRF_1$ (*i.e*, $p_2 = 2$, $q_2 = 3$ and $p_3 = 3$, $q_3 = 4$) would provide 33 possible combinations.

This example shows how our dealiasing process works through the following steps: i) Calculate the first term of (14), at any pixel, from the Doppler images $V_{D_i}(i \geq 2)$; ii) Determine the corresponding Nyquist numbers (n_{N_i}) using a lookup table (such as Table I); iii) Deduce the unambiguous Doppler velocity using a weighted mean issued from expression (10):

$$V_D^u = \frac{\sum_i \frac{q_i}{p_i} V_D^u}{\sum_i \frac{q_i}{p_i}} = \frac{\sum_i \frac{q_i}{p_i}(V_{D_i} + 2 n_{N_i} V_{N_i})}{\sum_i \frac{q_i}{p_i}}. \tag{16}$$

Coming back to the abovementioned dual-PRF scheme ($p_1 = 1$, $q_1 = 1$, $p_2 = 3$, $q_2 = 4$), two Doppler fields are available (V_{D_1} and V_{D_2}). The lookup table is used as follows: i) Calculate $\text{nint}(2(V_{D_2} - V_{D_1})/V_{N_1})$ everywhere (1st column of Table I); ii) Determine n_{N_1} and n_{N_2}. For example, if $\text{nint}(2(V_{D_2} - V_{D_1})/V_{N_1}) = -2$, then $n_{N_1} = 1$ and $n_{N_2} = 2$ (2nd row of Table I); iii) Deduce the unambiguous Doppler velocity from (16). For this same pixel, we have $V_D^u = [(V_{D_1} + 2 V_{N_1}) + 4/3 (V_{D_2} + 4 V_{N_1})] / (1 + 4/3)$.

Theoretically, the larger the integers p_i, the better is the Nyquist interval extension, as mentioned earlier (see (9)). Large p_i, however, can lead to erroneous Nyquist numbers, as we will now explain. Relating the measured Doppler velocities (V_{D_i}) to the expected Doppler velocities ($\widetilde{V}_{D_i}$) by $V_{D_i} = \widetilde{V}_{D_i} + \epsilon_i$, where ϵ_i is the measurement error, (14) becomes:

$$\text{nint}\left(q_i \frac{\widetilde{V}_{D_i} - \widetilde{V}_{D_1} + \epsilon_i - \epsilon_1}{2 V_{N_1}}\right) = \text{nint}\left(q_i \frac{\widetilde{V}_{D_i} - \widetilde{V}_{D_1}}{2 V_{N_1}} + \right.$$
$$\left. q_i \frac{\epsilon_i - \epsilon_1}{2 V_{N_1}}\right) = n_{N_1} q_i - n_{N_i} p_i. \tag{17}$$

Since $\left(q_i \frac{\widetilde{V}_{D_i} - \widetilde{V}_{D_1}}{2 V_{N_1}}\right)$ is an integer $(= n_{N_1} q_i - n_{N_i} q_i)$, (17) remains true as long as

$$\max\left|q_j \frac{\epsilon_j - \epsilon_1}{2 V_{N_1}}\right| < 0.5 \; i.e., \; \max|q_i(\epsilon_i - \epsilon_1)| < V_{N_1}. \tag{18}$$

The variance of the Doppler velocity estimate is proportional to the pulse repetition frequency [29]. Therefore, assuming from

(8) that $\epsilon_i \sim \sqrt{p_i/q_i}\ \epsilon_1$ and that ϵ_i is independent from ϵ_1, we obtain the sufficient condition

$$(\sqrt{p_i q_i} + q_i) \max |\epsilon_1| < V_{N_1}. \qquad (19)$$

Inequality (19) shows that, for a given error distribution ϵ_1, both p_i and q_i cannot be too large to ensure the validity of expression (14) in most conditions. Because $p_i < q_i$ and p_i and q_i are relatively prime (for $i > 1$), it is convenient to choose $q_i = p_i + 1$, so that q_i is as small as possible. In situations where Doppler measurements errors are relatively high (low SNR, weakly correlated successive signals, low central frequency, low fractional bandwidth), it would be recommended not to use large p_i values. In our experimental studies, we used the ratios $p_i/q_i = 2/3$ and $3/4$. These values are common in Doppler radar and usually do not exceed $6/7$ [28]. How the p_i/q_i may influence the dealiasing process was investigated *in vitro*.

B. In Vitro Models—Spinning Disc and Free Jet Flow

We first tested staggered multiple-PRF ultrafast color Doppler on a 10-cm-diameter tissue-mimicking disc. This disc was mounted on a step motor assembly allowing control of its rotational speed. The phantom rotated at angular velocities ranging from 20 to 500 revolutions per minute (with an increment of 20), which gave a maximum outer speed of $\sim$ 2.6 m/s. The disc was insonated with diverging wavefronts transmitted by a phased-array transducer (see following subsection). To obtain more realistic Doppler data, we then completed the *in vitro* analysis with a free water jet flow generated by a sharp-edged circular orifice plate (inner diameter of $\sim$ 13 mm). A low-concentration of cornstarch particle suspension mimicked the backscattering effect of red blood cells. The set-up included a controllable centrifugal pump (Micropump 75211-62, Cole-Parmer, Canada) and an electromagnetic flowmeter (Omega, FMG203, Canada). The flow rate was varied from 3.5 to 5.5 liters per minute (maximum jet speed of $\sim$ 1.15 m/s). The phased-array transducer was positioned parallel to the jet and the flow was directed towards the transducer.

C. In Vitro Acquisition—Ultrasound Sequences

We used a Verasonics research scanner (V-1-128, Verasonics Inc., Redmond, WA) to carry out the *in vitro* experiments. A 2.5-MHz phased-array transducer (ATL P4-2, 64 elements, pitch = 0.32 mm) was used to transmit diverging circular wavefronts using a full aperture. Diverging wavefronts were transmitted by a virtual source located behind the ultrasound transducer [30]. The location of this source was defined by the angular width and tilt of the region of interest (tilt = $0°$ *in vitro*), as well as the aperture of the transducer (see Fig. 2). The angular widths were $90°$ for the spinning disc, and $30°$ for the flow jet. An ensemble of long ultrasound pulses (6 wavelengths) was emitted at two or three staggered PRF (see Fig. 1) to provide color Doppler estimates. The *in vitro* rotating disc was imaged using a staggered triple-PRF pulsing sequence with $PRF_1 = 5000$ Hz, $PRF_2 = 2/3\ PRF_1 = 3333$ Hz, and $PRF_3 = 3/4\ PRF_1 = 3750$ Hz (Fig. 1, 3rd sequence). The corresponding extended Nyquist velocity (9) was $6V_{N_1} = 6 \times 0.75 = 4.5$ m/s. The free jet flow was
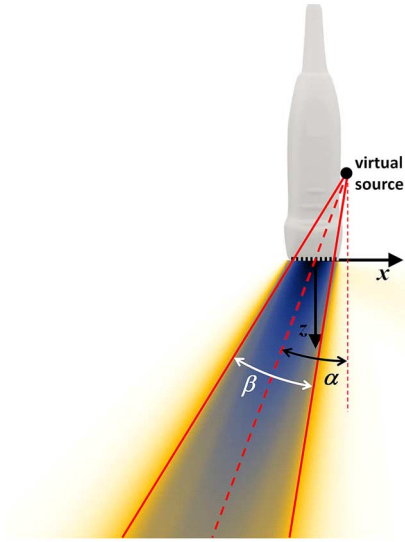

Fig. 2. Diverging circular wave transmission. The virtual source (black dot) is located behind the ultrasound phased-array transducer. Transmission delays applied to the piezoelectric elements are defined by the angular width β and tilt θ of the region-of-interest (shaded zone) and the transducer aperture.

insonated using a dual-PRF scheme with $PRF_1 = 5500$ Hz and $PRF_2 = 2/3\ PRF_1 = 3666$ Hz (Fig. 1, 2nd sequence) whose extended Nyquist velocity was $2V_{N_1} = 2 \times 0.8 = 1.6$ m/s.

D. Effect of (p/q) on Dealiasing—Spinning Disc

Equation (19) states that p and q must not be too large to avoid erroneous Nyquist numbers. To investigate the effect of (p/q) on the dealiasing process, the spinning disc was also imaged in Doppler mode using eleven dual-PRF schemes with $PRF_2 = p/(p+1)PRF_1$. A single rotation speed of 400 revolutions per minute (*i.e.* maximum outer speed of $\sim$ 2.1 m/s) was tested for this investigation. We choose $p = 2, 3 \ldots 11, 12$. As previously indicated, the angular width of the emitted pressure field was $90°$ and PRF_1 was 5000 Hz.

E. In Vivo Validation—Ventricular Filling

To test the *in vivo* feasibility of staggered multiple-PRF ultrafast color Doppler, we scanned the left heart of a 30-year-old healthy volunteer with the Verasonics research scanner and the 2.5-MHz phased-array transducer. To obtain a 5-chamber view, we carried out ultrafast acquisitions along the long-axis view from the apical position. The angular width was $90°$. To perform duplex scanning, 16 tilted transmissions (from $-25°$ to $+25°$) were emitted at 3000 Hz using short ultrasound pulses (2 wavelengths) to create B-mode images from coherent compounding (see Table II). Subsequently, an ensemble of 33 (*i.e.* 2×16 pairs) long ultrasound pulses (8 wavelengths) was emitted at two staggered PRF (see Fig. 1) to provide color Doppler estimates. The PRFs were $PRF_1 = 3000$ Hz and $PRF_2 = 2/3\ PRF_1 = 2000$ Hz (Fig. 1, 2nd sequence), which gave an extended Nyquist velocity of $2V_{N_1} = 2 \times 0.45 = 0.90$ m/s. No coherent compounding was performed in Doppler mode (tilting angle = $0°$). The reference PRF was intentionally decreased (3000 instead of 4000–5000 Hz) to induce significant intraventricular Doppler aliasing in the normal heart. To deduce

TABLE II
CIRCULAR WAVE IMAGING PARAMETERS *(IN* VIVO)

Parameter	B-mode	Doppler
Probe	ATL P4-2 (phased array)	
Elements	64	
Center frequency	2.5 MHz	
Pitch	0.3 mm	
PRF	3000 Hz	3000 / 2000 Hz (dual)
Packet size	16	33 (2×16 pairs)
Cycles	2	6
Width	90°	90°
Tilt	-25° to 25°	0°

the image rate, let N_D represent the number of image pairs to obtain each Doppler field. The ensemble length is thus $(2N_D + 1)$ or $(3N_D + 1)$ for a dual- or triple-PRF scheme, respectively. Let N_B denote the number of transmissions to generate one coherently compounded grayscale image. The time required to produce one duplex image is thus $T_{\text{duplex}}(n_{\text{PRF}}) = \left(N_B + N_D \sum_{i=1}^{n_{\text{PRF}}} q_i/p_i\right)/\text{PRF}_1$, with n_{PRF} equals 1, 2 or 3, for single-, dual- or triple-PRF emission, respectively. In our *in vivo* experiments ($N_B = 16$, $N_D = 16$, $p_1 = 1$, $p_2 = 2$, $q_1 = 1$, $q_2 = 3$), T_{duplex} was 18.6 ms, which gave 54 duplex images/s. The experimental protocol was approved by the human ethical review committee of the University of Montreal Hospital Research Center. The volunteer signed an informed consent form approved by the local ethics committee before the exam. Approval by Health Canada was also obtained for using the experimental ultrasound scanner in volunteers.

F. Doppler Velocity Estimation

Acquired RF data were sampled at 10 MHz, IQ-demodulated then dynamically focused in reception by using a standard diffraction summation (delay-and-sum) [31] technique programmed on graphics processing units (GPU). No apodization was used either in transmission or reception. We beamformed and post-processed the IQ (in-phase/quadrature) data offline. Doppler velocities were estimated from the IQ signals after clutter filtering (clutter filtering was necessary only *in vivo*, see next paragraph) as follows. Two (dual-PRF) or three (triple-PRF) Doppler fields (V_{D_1}, V_{D_2} and V_{D_3}) were estimated from clutter-filtered beamformed IQ signals using the 2-D auto-correlator proposed by Loupas *et al.* [32]. We calculated each Doppler field independently using the pulse pairs corresponding to the respective pulse repetition periods PRP_1, PRP_2 and PRP_3 (see Fig. 1). For the *in vitro* experiments, the staggered slow-time sequences were composed of a packet of 39 (dual-PRF) or 58 (triple-PRF) received pulses, which correspond to 19 pulse pairs for each individual PRF. For the *in vivo* experiments, the staggered slow-time sequences were reduced to 33 (dual-PRF) transmitted pulses, which correspond to 16 pulse pairs for each individual PRF. We then deduced the left hand side terms of (14) and determined the related Nyquist numbers (n_{N_i}) using the predefined lookup table (see Table I for an example). The dealiased Doppler fields were obtained from the weighted mean (16). Some few remaining errors were removed with a multi-pass 3×3 spatial median filter. This filter helped to remove a few isolated outliers or very

small clusters of outliers. The power Doppler fields were also determined *in vivo* from the complete slow-time sequences. Power Doppler was used to define the regions of interest within the color Doppler images.

G. Adaptive Regression Clutter Filter

Clutter mostly refers to strong tissue echoes that might interfere with blood flow Doppler signals. If not adequately reduced, it might produce strongly biased Doppler velocities. In most cases, the clutter signal is narrowband with center frequency close to zero; it can thus generally be curtailed by a high-pass filter. FIR or IIR (finite/infinite response) filters and polynomial regression are the most common (and simplest) clutter rejection algorithms for color Doppler [33]. FIR and IIR require the signals to be uniformly sampled and are not adapted for our multiple-PRF schemes. Other filters based on conversion into principal components (eigenfilters) also work with regularly-spaced signals only [34]. To eliminate clutter components, we high-pass filtered the IQ signals using orthogonal polynomial regression since it can deal with irregularly sampled signals. Polynomial regression filters assume that clutter echoes are of high amplitude, vary slowly compared to blood signals, and can be approximated by a polynomial determined in a least-squares sense: the polynomial clutter component is subtracted from the original Doppler signal to retrieve the blood flow contribution. Polynomials of 1st- up to 4th-degree were proposed in the literature [35]. For a given packet length, the polynomial degree controls the transition band and the cut-off frequency of the clutter filter [33]. A fixed polynomial degree thus results in homogeneous clutter filtering. Fixing the polynomial degree, however, may be suboptimal since the clutter-to-blood spectral separation often varies spatially and temporally. A too low degree may thus overlook clutter, whereas a too high degree may degrade blood signal. To address this issue, we used the Akaike's information criterion (AIC) [36]. The AIC is a criterion for model selection; it allows one to find which model (from a set of models) best fits the given data. The AIC trades off the statistical goodness-of-fit against the number of parameters that have to be estimated to achieve this fit [36]. The model with the lowest AIC hence is considered the best possible choice among all models specified. The AIC is particularly well adapted to least-squares estimation [37]. When the sample size is small, it is recommended to use the corrected AIC. In the special case of polynomial regression with normally distributed errors, the corrected AIC is given by [37]:

$$\text{AIC}_C = n\left\{\ln\left(\frac{\text{RSS}}{n}\right) + \frac{n + m + 1}{n - m - 3}\right\}. \quad (20)$$

In (20), n corresponds to the sample size (*i.e.* the packet length), m is the degree of the fitting polynomial, and RSS is the sum of squares of the residuals between the original data and the polynomial model. The first term in the brackets is related to the goodness-of-fit; it decreases logarithmically when m increases. The second term represents a penalty term; it increases exponentially with increasing m. AIC_C reaches a global minimum in $m \in [1, n - 2]$. In the context of Doppler imaging, we assumed that the blood Doppler signal was mainly contained in the residuals of the full Doppler signal. In this study, instead of
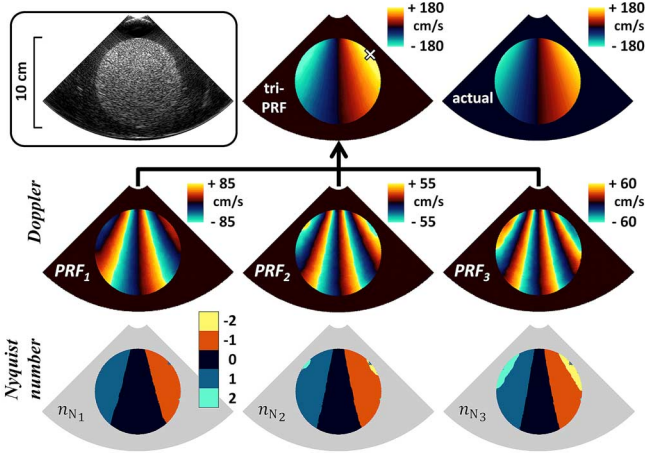
Fig. 3. Triple-PRF ultrafast Doppler in the spinning disc. *Second row*: masked color Doppler images corresponding to the pulse pairs emitted at PRF_1 (5000 Hz), PRF_2 (3333 Hz) and PRF_3 (3750 Hz), respectively. *Third row*: maps of the corresponding Nyquist numbers which were used to reconstruct the unaliased Doppler field (top-center) from the Doppler velocity fields of the 2nd row by using (16). *Top-left*: B-mode image obtained using one diverging circular beam with a six-cycle pulse. *Top-center and top-right*: unaliased color Doppler image using the triple-PRF approach in comparison with the ground-truth radial velocities. These images were obtained at 340 rotations per minute. The white X-cross (top-center) is the location of maximal Doppler velocity (see Fig. 4).

using a fixed degree [38], and to make the polynomial regression filter spatially adaptive, we selected (*for each single slow-time ensemble*) the polynomial model which minimized the corrected AIC (20). The AIC-based polynomial degree was thus

$$m_{AIC} = \arg\min_m \{AIC_C\}$$
$$= \arg\min_m \left\{ \ln\left(\frac{RSS}{n}\right) + \frac{2n-2}{n-m-3} \right\}. \quad (21)$$

We sought this optimal polynomial degree in the ensemble $\{6, 8, 10, 12, 14, 16\}$ for the *in vivo* analyses.

III. RESULTS

A. In Vitro Spinning Disc

Although large aliased areas were present in the single-PRF Doppler fields (see an example at 340 rpm in Fig. 3, second row), the triple-PRF approach allowed full dealiasing of Doppler velocities (Fig. 3, top center). The Nyquist numbers determined by the lookup table of the Appendix were ranged between -2 and 2 (Fig. 3, third row). For each rotational speed (see Fig. 4), we compared the Doppler velocity at the location of the maximum positive radial velocity (white cross on Fig. 3) with the ground-truth maximum speed given by ωR, where ω and R stand for the angular velocity and the radius of the disc. With a single PRF ($PRF_1 = 5000$ Hz), as expected from (1), a first aliasing occurred at ~ 0.75 m/s, and a second at $\sim (0.75 + 2 \times 0.75) = 2.25$ m/s (Fig. 4, diamonds). A dual-PRF approach (with $PRF_1 = 5000$ Hz, and $PRF_2 = 2/3 \, PRF_1 = 3333$ Hz) extended the unambiguous velocity to twice the original velocity range (Fig. 4, empty dots), as predicted by (9). Because the extended Nyquist
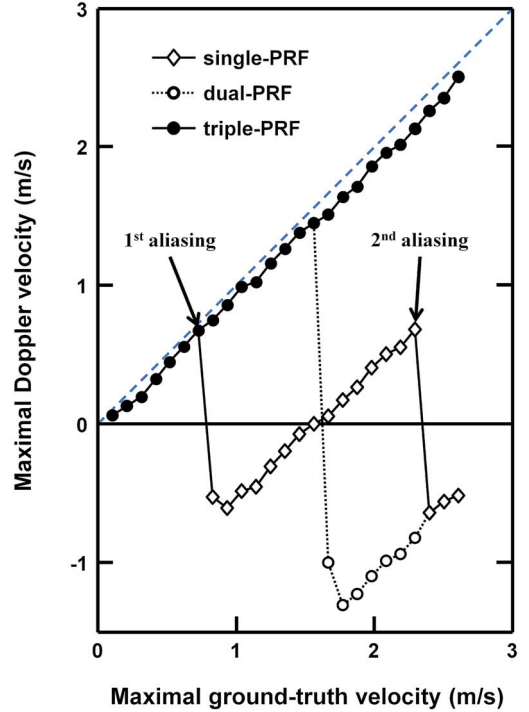

Fig. 4. Ultrafast Doppler in the spinning disc: maximal velocities; Doppler vs. ground-truth. The "maximal" Doppler velocity is the Doppler velocity at the location of the peak positive radial velocity. The diamonds represent the Doppler velocities measured in the spinning disc with a conventional single-PRF approach (at $PRF_1 = 5000$ Hz). Aliasing occurred above 0.75 and 2.25 m/s (see also Fig. 3, 2nd row). The empty dots depict the dual staggered PRF scheme (2nd sequence in Fig. 1), where the second PRF_2 was $2/3 \, PRF_1 = 3750$ Hz. Aliasing occurred above 1.5 m/s. The full dots illustrate the Doppler velocities with the triple-PRF approach. No aliasing was present. The dashed line is the identity line.

velocity was 4.5 m/s, no aliasing occurred with the triple-PRF approach within the velocity range of the experiments (Fig. 4, full dots). Good accuracy and precision were found between the triple-PRF peak Doppler velocities and the ground-truth maximal velocities (Fig. 4, full dots, $y = 0.96x - 0.06$, $r^2 > 0.99$). The absolute global error measured in the masked Doppler velocity field (*i.e.* on the whole disc) was given by the RMSE (root-mean-square error between Doppler and ground-truth radial velocities). The NRMSE (normalized RMSE) was defined as the RMSE normalized to the root-mean-square of the ground-truth values. The RMSE increased linearly with the rotational speed (Fig. 5, diamonds) but remained small (< 0.1 m/s) in comparison with the maximum velocities. The NRMSE decreased exponentially and was smaller than 8% for the highest rotation speeds (Fig. 5, solid circles).

B. In Vitro Spinning Disc: Effect of (p/q) on Dealiasing

With a dual-PRF transmission using $PRF_1 = 5000$ Hz and $PRF_2 = p/(p+1)PRF_1$, the root-mean-square errors were alike for $p = 2, 3, 4, 5$ (Fig. 6). The errors, however, increased linearly when $p > 5$, i.e., when PRF_2 became closer to PRF_1. In such conditions, an increased number of erroneous Nyquist numbers were observed, thus leading to suboptimal dealiasing. These results confirm that the integers p and q must not be too large, as explained by (17) to (19).
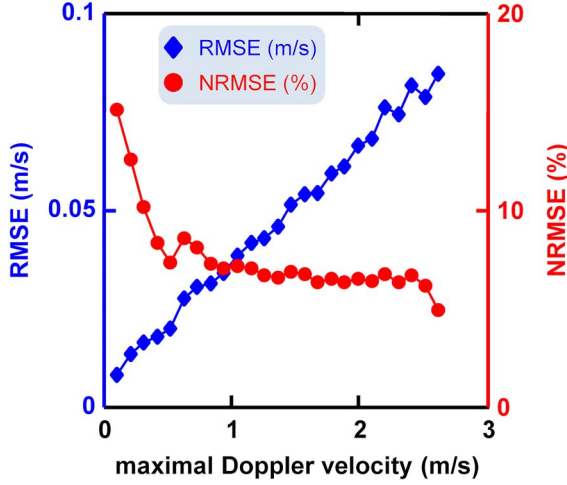
Fig. 5. Ultrafast Doppler in the spinning disc: total errors (on the whole disc). Global root-mean-square error (RMSE, diamonds) and normalized RMSE (NRMSE, solid circles) returned by the triple-PRF approach (see 1st row in Fig. 3, top-center).
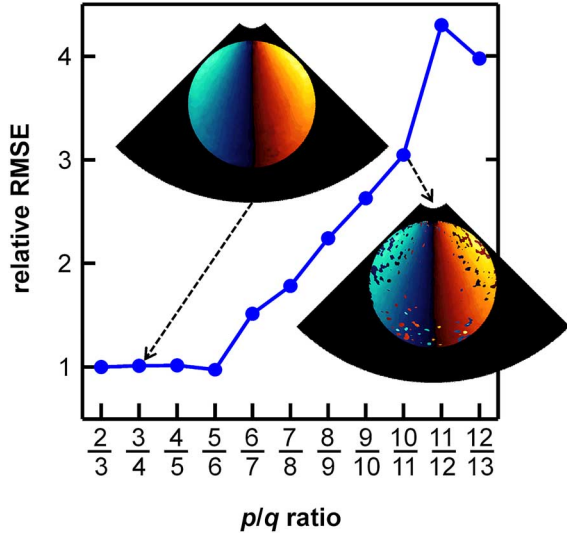

Fig. 6. Effect of (p/q) on dealiasing. Global root-mean-square error (RMSE) of the dealiased Doppler field (relative to value at $p/q = 2/3$). Doppler velocities were measured in the spinning disc with a dual-PRF approach ($\mathrm{PRF}_1 = 5000\ \mathrm{Hz}; \mathrm{PRF}_2 = p/q\ \mathrm{PRF}_1$). The insets show the Doppler velocities dealiased by the proposed method for $p/q = 3/4$ and $p/q = 10/11$. Note the spurious velocities when p/q is close to one (see also (19)).

C. In Vitro Flow Jet

The dual-PRF approach allowed full disambiguation of Doppler velocities in the free flow jet (Fig. 7, 1st row). The Nyquist numbers used to dealias the jet Doppler fields were mostly 0 (no aliasing) and $+1$ (positive aliasing). The $+1$ Nyquist numbers were expectedly present in the jet core (Fig. 7, 2nd row). For a free jet generated by a sharp-edged thin orifice plate, the velocity at the vena contracta (*i.e.* the maximum jet velocity) is approximately given by:

$$V_{\max} \approx \frac{Q}{0.6\,A}, \tag{22}$$

where Q is the flow rate and A represents the aperture area [39]. We compared this theoretical velocity with the maximum
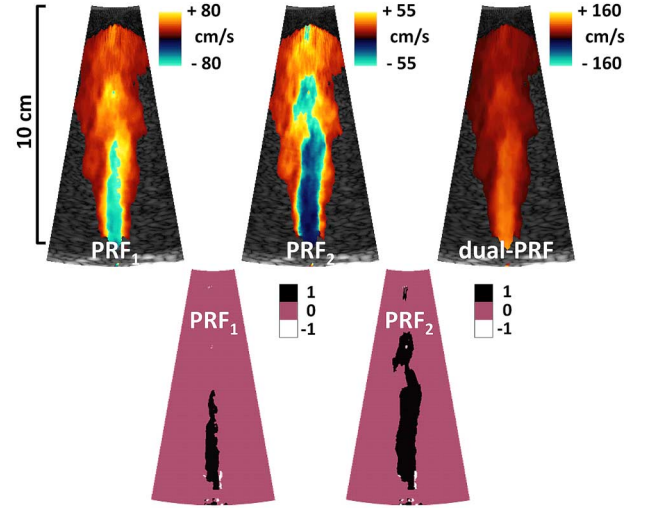

Fig. 7. Dual-PRF ultrafast Doppler in the free flow jet. *First row, Left and Center*: color Doppler images corresponding to the pulse pairs emitted at PRF_1 (5500 Hz) and PRF_2 (3666 Hz), respectively. *First row, Right*: dealiased color Doppler image using the dual-PRF approach. *Second row*: maps of the corresponding Nyquist numbers which were used to reconstruct the unaliased Doppler field (top-right) from the Doppler velocity fields of the 1st row by using (16). The flow rate was here 4.9 L/min.
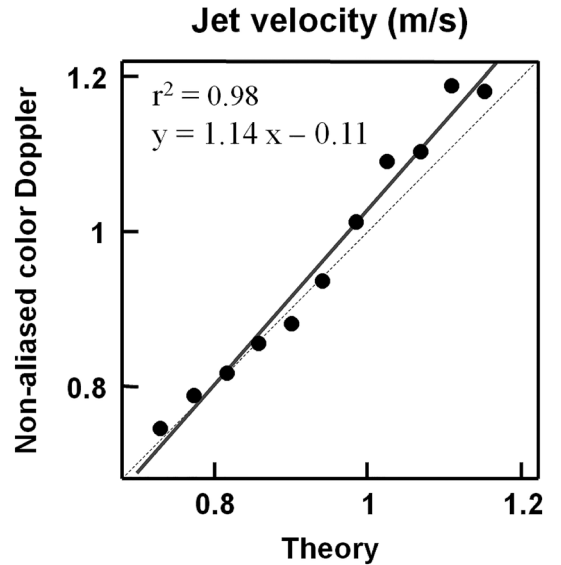

Fig. 8. Jet velocity: color Doppler vs. theoretical. A coefficient of determination of $r^2 = 0.98$ was observed between the maximum Doppler velocity and the theoretical jet velocity estimated from (22). The dashed line is the identity line; the solid line is the regression line.

Doppler velocity issued from the dual-PRF ultrasound sequence (Fig. 8). Good accuracy and precision were obtained (regression line: $y = 1.14x - 0.11$; coefficient of determination: $r^2 = 0.98$).

D. In Vivo Left Ventricle

The dual-PRF approach was also effective *in vivo* in the left heart (Fig. 9). Since we decreased the maximum PRF (*i.e.,* $\mathrm{PRF}_1 = 3$ kHz) intentionally (see Section II-E), significant aliasing was present in the single-PRF Doppler images. As expected, aliasing was more pronounced with PRF_2 since PRF_2 was smaller than PRF_1. Although aliasing was present in the single-PRF Doppler fields (Fig. 9), the dual-PRF approach
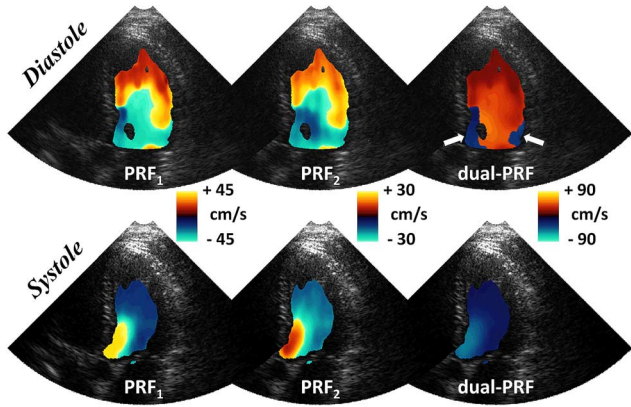
Fig. 9. Color flow imaging in the left ventricle (five chamber view) with the staggered multi-PRF ultrafast technique. *Left*: Aliased color Doppler map obtained with a single-PRF transmission scheme, with $\text{PRF}_1 = 3$ kHz. *Middle*: idem, with $\text{PRF}_2 = 2$ kHz. *Right*: De-aliased color Doppler map obtained with a staggered dual-PRF transmission scheme ($\text{PRF}_1 = 3$ kHz, $\text{PRF}_2 = 2$ kHz). Thick white arrows: backflow due to the mitral leaflets or residual clutter? See also the corresponding online movie.
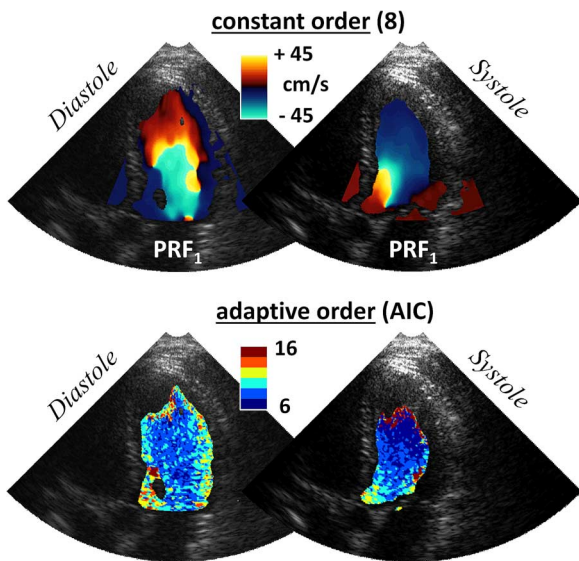

Fig. 10. AIC-based adaptive clutter filter. *Top*: Color Doppler estimates obtained after filtering the IQ Doppler ensemble with an 8th order polynomial regression clutter filter. The clutter is not totally removed; see Fig. 9, 1st column, for comparison. *Bottom*: Polynomial orders returned by the AIC minimization criterion. These orders were used in the polynomial regression filter. The corresponding Doppler fields are in Fig. 9.

doubled the Nyquist velocity and allowed disambiguation of Doppler velocities. The AIC minimization criterion helped to adapt polynomial clutter filtering spatially (Fig. 10). Whereas a fixed polynomial 8th order returned Doppler artifacts near the myocardium and the outflow tract (Fig. 10, top), the adaptive regression filter showed that orders up to 14 (Fig. 10, bottom) were necessary to reconstruct visually-consistent Doppler fields (Fig. 9, 1st column). These results show that the staggered multiple-PRF approach might be well adapted to ultrafast color Doppler with circular ultrasound beams. A cineloop showing the whole heart cycle is available online.

IV. DISCUSSION

Color Doppler presently remains a visualization means of detecting blood flow anomalies. Original qualitative tools have been proposed to better decipher intravascular and intracardiac flow dynamics [2], [3], [8]. However, they may be limited by aliasing and/or low frame rates. In this work, we proposed to transmit large wavefronts in a staggered alternating way to get alias-free Doppler velocity fields at high frame rates. The Nyquist numbers were recovered using a simple algorithm to dealias the Doppler velocities. Although further work is needed to validate our approach in additional *in vivo* situations, our *in vitro* and *in vivo* experiments showed that the staggered multiple-PRF approach could upgrade quantitative color Doppler.

A. Alias-Free Methods for Color Doppler

Numerous tools were proposed to unwrap images in medical ultrasound and other fields. Existing post-processing unwrapping techniques for removing aliasing were briefly described in the introduction. Alternative direct approaches were developed to estimate blood Doppler velocities beyond the Nyquist range. The time-domain cross-correlation method is the commonest one of them [40]. It estimates time-shift rather than phase-shift and is generally exempt from aliasing. This approach has been shown to achieve at least the same precision as the phase-domain auto-correlation [41]. The temporal cross-correlation and peak-fitting processes, however, make this approach more computationally expensive [42]. To keep advantage of the alias-free property of the cross-correlation method at a lower computational cost, the auto-correlation method was extended to take amplitude information into account [43]. The extended auto-correlation method was shown to have a similar performance as that of the standard cross-correlation method [43], which potentially makes it a good candidate for unaliased Doppler estimation. In this study, we used the classical phase-domain auto-correlator [32] to determine the Doppler velocities. Since this is a phase shift which is measured, this narrow-band estimator is subject to aliasing. We showed however that staggered multiple-PRF schemes can return unaliased Doppler images, as long as blood speed does not exceed the extended Nyquist velocity given by (9). With the $2/3$–$3/4$ triple-PRF scheme tested in the spinning disc, it was possible to sextuple the original Nyquist limit. In all configurations, we removed aliasing significantly, both *in vitro* and *in vivo*. The multiple-PRF technique has the ability to return alias-free Doppler fields with a very low computational complexity in comparison with the abovementioned methods. Multiple-PRF transmissions in color Doppler are made possible by ultrafast ultrasound imaging.

B. Advantages of Ultrafast Color Doppler

Conventional 2-D Doppler imaging of the whole left ventricle generally offers only ~ 10 duplex (Doppler + B-mode) images per heart cycle, which is insufficient for characterizing the intraventricular blood flow. Ultrafast ultrasound imaging can provide high-frame-rate data acquisition using transmissions of plane or diverging waves. In the context of ultrasound cardiac imaging, note that the attributive adjective "ultrafast" must be considered as a hyperbole since it is not yet feasible

to get thousands or even hundreds of high-quality duplex images per second. However, it is becoming possible to obtain a sufficient number of high-quality images in a single heart beat. In our *in vivo* study, even with a PRF as low as 3000 Hz, we reached > 50 duplex frames per heart cycle. We thus obtained a five-fold increase in comparison with conventional Doppler imaging. With a 4000-5000 PRF sequence, we would have reached 70-90 Doppler frames per cycle. This is more than enough to decipher the main patterns (excluding turbulence) of the intracardiac blood flow. The other side of the coin is that the large ultrasound wavefronts generate significant clutter.

C. Clutter Removal

The main challenge in Doppler imaging is the suppression of low-frequency high-amplitude clutter. To deal with the small unevenly spaced slow-time ensembles, we opted for the polynomial regression filter. Our results tend to show that this filter could be well adapted to the dual- and triple-PRF schemes. When coupled with the AIC minimization criterion, it became spatially adaptive and reduced biases due to clutter filtering. Further exhaustive *in vitro* and *in vivo* studies, however, are required to investigate the velocity bias introduced by polynomial regression clutter filtering with such staggered sequences. Indeed, non-stationary clutter might become significant due to non-uniform slow-time sampling [44]. To complicate matters, cardiac color Doppler is more sensitive to clutter when large (instead of focused) wavefronts are transmitted. The presence of high-amplitude clutter represents, for now, the weakest part of cardiac Doppler imaging with unfocused waves. Clutter filtering has long been the subject of a number of investigations in focused Doppler imaging [33], [35]. More investigations have to be made to further improve clutter filtering for plane or circular wave imaging. Eigen-based filters or other filters developed for staggered PRF schemes in meteorology [45], [46] could be tested. A possible comprehensive *in vivo* validation could be provided by comparing Doppler velocities derived from the proposed method with those obtained from aliasing-free techniques based on speckle tracking [47].

D. Aliasing: Helpful or Harmful?

The main objective of this study was to remove aliasing in color Doppler imaging. It exists situations, however, where aliasing is valuable. For example, color Doppler aliasing helps to visualize flow jets in ventricular septal defects or valvular diseases. It can also allow estimating the regurgitant flow in mitral, tricuspid or aortic regurgitation using the PISA (proximal isovelocity surface area) method. Another technique where aliasing is required is the measure of the transmitral flow propagation velocity for the assessment of the left ventricular rapid filling phase. In other recent echocardiographic tools, such as vector flow mapping [2], Doppler vortography [3] or intraventricular pressure gradient assessment [48], aliasing must be removed. The proposed multi-PRF approach could be therefore well adapted under the condition that no valvular or septal anomaly is present. Indeed, to work correctly, the flow must be quasi-stationary during the time required to register one multiple-PRF slow-time ensemble. This situation is not encountered in highly spatially and/or temporally fluctuating flows such as in valvular regurgitation or stenosis. Regurgitant jets are turbulent jets that can contain high-velocity and high-acceleration components [49]. This may result in rapidly varying aliased Doppler velocities, in which case, the multiple-PRF staggered method would be defective. Further *in vitro* analyses would be necessary to determine the practical limits of this technique.

V. CONCLUSION

The staggered multiple-PRF emission scheme for ultrafast color Doppler successfully extended the Nyquist limit *in vitro* and *in vivo*. Clutter filtering by adaptive polynomial regression appeared suited for the proposed strategy based on non-uniform slow-time sampling. Staggered multiple-PRF ultrafast color Doppler could thus be a method of choice for developing quantitative clinical tools based on color Doppler imaging.

APPENDIX

Demonstrations of Expressions (4), (12) and (15):

We first aim at demonstrating expression (4) of the Nyquist number. Due to aliasing, Doppler velocities can have no absolute values above the Nyquist velocity, so that:

$$V_D = (V_D^u + V_N)(\mod(2V_N)) - V_N. \tag{A1}$$

By definition of the congruence function, $m \mod(n) = m - n \, \text{floor}(m/n)$. Thus (A1) becomes

$$V_D = (V_D^u + V_N) - 2V_N \, \text{floor}\left(\frac{V_D^u + V_N}{2V_N}\right) - V_N, \tag{A2}$$

which can be rewritten as

$$V_D = V_D^u - 2 \, \text{floor}\left(\frac{V_D^u + V_N}{2V_N}\right) V_N. \tag{A3}$$

This proves (4). We now aim at demonstrating expression (12). Inequality (11) gives:

$$-kV_{N_1} < V_D^u < kV_{N_1}. \tag{A4}$$

Adding V_{N_i} then dividing by $(2V_{N_i})$ results in

$$-\frac{kV_{N_1}}{2V_{N_i}} + \frac{1}{2} < \frac{V_D^u + V_{N_i}}{2V_{N_i}} < \frac{kV_{N_1}}{2V_{N_i}} + \frac{1}{2}, \tag{A5}$$

which, from (8), can be rewritten as

$$-\frac{k\,q_i}{2p_i} + \frac{1}{2} < \frac{V_D^u + V_{N_i}}{2V_{N_i}} < \frac{k\,q_i}{2p_i} + \frac{1}{2}. \tag{A6}$$

It can be verified that $a \le x < b \Rightarrow \text{floor}(a) \le \text{floor}(x) \le \text{ceiling}(b-1)$. Therefore (A6) gives

$$\text{floor}\left(-\frac{k\,q_i}{2p_i} + \frac{1}{2}\right) \le \text{floor}\left(\frac{V_D^u + V_{N_i}}{2V_{N_i}}\right)$$
$$\le \text{ceiling}\left(\frac{k\,q_i}{2p_i} - \frac{1}{2}\right). \tag{A7}$$

Since $\forall x$, $\text{floor}(-x) = -\text{ceiling}(x)$, (A4) becomes

$$\left| \text{floor}\left(\frac{V_D^u + V_{N_i}}{2V_{N_i}}\right) \right| \le \text{ceiling}\left(\frac{k\,q_i}{2p_i} - \frac{1}{2}\right). \tag{A8}$$

From the definition of the Nyquist number (4), (A8) leads to inequality (12)

$$|n_{\text{N}_i}| \le \text{ceiling}\left(\frac{k\,q_i}{2p_i} - \frac{1}{2}\right). \tag{A9}$$

We finally aim at demonstrating the inequality (15). We have, by definition of the Nyquist velocity

$$\forall i, |V_{\text{D}_i}| \le V_{\text{N}_i}. \tag{A10}$$

The triangle inequality leads to

$$|V_{\text{D}_i} - V_{\text{D}_1}| \le V_{\text{N}_i} + V_{\text{N}_1}, \tag{A11}$$

which can be rewritten, after division by $2V_{\text{N}_1}$, as

$$\left|\frac{V_{\text{D}_i} - V_{\text{D}_1}}{2V_{\text{N}_1}}\right| \le \frac{V_{\text{N}_i}}{2V_{\text{N}_1}} + \frac{1}{2}. \tag{A12}$$

Using equalities (8) and (13), because $q_i > 0$, we obtain the inequality (15)

$$|n_{\text{N}_1} q_i - n_{\text{N}_i} q_i| \le \frac{1}{2}(p_i + q_i). \tag{A13}$$

REFERENCES

[1] T. Uejima *et al.*, "A new echocardiographic method for identifying vortex flow in the left ventricle: Numerical validation," *Ultrasound Med. Biol.*, vol. 36, no. 5, pp. 772–788, 2010.

[2] D. Garcia *et al.*, "Two-dimensional intraventricular flow mapping by digital processing conventional color-Doppler echocardiography images," *IEEE Trans. Med. Imag.*, vol. 29, no. 10, pp. 1701–1713, Oct. 2010.

[3] F. Mehregan *et al.*, "Doppler vortography: A color Doppler approach to quantification of intraventricular blood flow vortices," *Ultrasound Med. Biol.*, vol. 40, no. 1, pp. 210–221, 2014.

[4] R. Ro *et al.*, "Vector flow mapping in obstructive hypertrophic cardiomyopathy to assess the relationship of early systolic left ventricular flow and the mitral valve," *J. Am. Coll. Cardiol.*, vol. 64, no. 19, pp. 1984–1995, 2014.

[5] J. Bermejo *et al.*, "Intraventricular vortex properties in nonischemic dilated cardiomyopathy," *Am. J. Physiol Heart Circ. Physiol.*, vol. 306, no. 5, pp. H718–H729, 2014.

[6] J. Udesen *et al.*, "High frame-rate blood vector velocity imaging using plane waves: Simulations and preliminary experiments," *IEEE Trans. Ultrason. Ferroelectr. Freq. Control*, vol. 55, no. 8, pp. 1729–1743, Aug. 2008.

[7] J. Bercoff *et al.*, "Ultrafast compound Doppler imaging: Providing full blood flow characterization," *IEEE Trans. Ultrason. Ferroelectr. Freq. Control*, vol. 58, no. 1, pp. 134–147, Jan. 2011.

[8] I. K. Ekroll *et al.*, "Simultaneous quantification of flow and tissue velocities based on multi-angle plane wave imaging," *IEEE Trans. Ultrason., Ferroelectr. Freq. Control*, vol. 60, no. 4, pp. 727–738, Apr. 2013.

[9] S. Ricci, L. Bassi, and P. Tortoli, "Real-time vector velocity assessment through multigate Doppler and plane waves," *IEEE Trans. Ultrason., Ferroelectr., Freq. Control*, vol. 61, no. 2, pp. 314–324, Feb. 2014.

[10] C. Papadacci, M. Pernot, M. Couade, M. Fink, and M. Tanter, "High-contrast ultrafast imaging of the heart," *IEEE Trans. Ultrason., Ferroelectr., Freq. Control*, vol. 61, no. 2, pp. 288–301, Feb. 2014.

[11] S. I. Nikolov and J. A. Jensen, "In-vivo synthetic aperture flow imaging in medical ultrasound," *IEEE Trans. Ultrason. Ferroelectr. Freq. Control*, vol. 50, no. 7, pp. 848–856, Jul. 2003.

[12] J. Provost *et al.*, "3D ultrafast ultrasound imaging in vivo," *Phys. Med. Biol.*, vol. 59, no. 19, pp. L1–L13, 2014.

[13] A. A. Pellett, W. G. Tolar, D. G. Merwin, and E. K. Kerut, "Doppler aliasing," *Echocardiography*, vol. 22, no. 6, pp. 540–543, 2005.

[14] D. C. Ghiglia and M. D. Pritt, *Two-Dimensional Phase Unwrapping: Theory, Algorithms, and Software*. New York: Wiley, 1998.

[15] S. Muth, S. Dort, I. A. Sebag, M. J. Blais, and D. Garcia, "Unsupervised dealiasing and denoising of color-Doppler data," *Med. Image Anal.*, vol. 15, no. 4, pp. 577–588, 2011.

[16] A. M. Yatchenko, A. S. Krylov, V. A. Sandrikov, and T. Y. Kulagina, "Regularizing method for phase antialiasing in color Doppler flow mapping," *Neurocomputing*, vol. 139, no. 0, pp. 77–83, 2014.

[17] R. J. Doviak, D. S. Zrnic, and D. S. Sirmans, "Doppler weather radar," *Proc. IEEE*, vol. 67, no. 11, pp. 1522–1553, Nov. 1979.

[18] D. Sirmans, D. Zrnic, and B. Bumgarner, "Extension of maximum unambiguous Doppler velocity by use of two sampling rates," in *17th Conf. Radar Meteorol.*, Seattle, WA, 1976, pp. 23–28.

[19] D. S. Zrnic and P. Mahapatra, "Two methods of ambiguity resolution in pulse Doppler weather radars," *IEEE Trans. Aerosp. Electron. Syst.*, no. 4, pp. 470–483, 1985.

[20] R. J. Doviak and D. S. Zrnic, *Doppler Radar and Weather Observations*. Mineola, NY: Courier Dover, 1993.

[21] H. Nishiyama and K. Katakura, "Non-equally-spaced pulse transmission for non-aliasing ultrasonic pulsed Doppler measurement," *J. Acoust. Soc. Japan. E*, vol. 13, no. 4, pp. 215–222, 1992.

[22] G. E. C. Nogueira, A. Ferreira, and J. T. Vidal, "A nonuniform sampled coherent pulsed Doppler ultrasonic velocimeter with increased velocity range," *IEEE Trans. Ultrason., Ferroelectr. Freq. Control*, vol. 46, no. 2, pp. 452–456, Mar. 1999.

[23] H. J. Nitzpon, J. C. Rajaonah, C. B. Burckhardt, B. Dousse, and J. J. Meister, "A new pulsed wave Doppler ultrasound system to measure blood velocities beyond the Nyquist limit," *IEEE Trans. Ultrason., Ferroelectr. Freq. Control*, vol. 42, no. 2, pp. 265–279, Mar. 1995.

[24] W. Bergen and S. Albers, "Two- and three-dimensional de-aliasing of Doppler radar velocities," *J. Atmospheric Oceanic Technol.*, vol. 5, no. 2, 1988.

[25] D. H. Evans, *Doppler Ultrasound: Physics, Instrumentation, and Clinical Applications*. New York: Wiley, 1989.

[26] J. E. Moller, E. Sondergaard, S. H. Poulsen, and K. Egstrup, "Pseudonormal and restrictive filling patterns predict left ventricular dilation and cardiac death after a first myocardial infarction: A serial color M-mode Doppler echocardiographic study," *J. Am. Coll. Cardiol.*, vol. 36, no. 6, pp. 1841–1846, 2000.

[27] S. L. Durden and C. L. Werner, "Application of an interferometric phase unwrapping technique to dealiasing of weather radar velocity fields," *J. Atmospheric Oceanic Technol.*, vol. 13, no. 5, pp. 1107–1109, 1996.

[28] P. Tabary, F. Guibert, L. Perier, and J. Parent-du-Chatelet, "An operational triple-PRT Doppler scheme for the French radar network," *J. Atmospheric Oceanic Technol.*, vol. 23, no. 12, pp. 1645–1656, 2006.

[29] J. A. Jensen, "Color flow mapping using phase shift estimation," in *Estimation of Blood Velocities Using Ultrasound*. Cambridge, U.K.: Cambridge Univ. Press, 1996, pp. 195–226.

[30] B. F. Osmanski, D. Maresca, E. Messas, M. Tanter, and M. Pernot, "Transthoracic ultrafast Doppler imaging of human left ventricular hemodynamic function," *IEEE Trans. Ultrason., Ferroelectr., Freq. Control*, vol. 61, no. 8, pp. 1268–1275, Aug. 2014.

[31] G. Montaldo, M. Tanter, J. Bercoff, N. Benech, and M. Fink, "Coherent plane-wave compounding for very high frame rate ultrasonography and transient elastography," *IEEE Trans. Ultrason. Ferroelectr. Freq. Control*, vol. 56, no. 3, pp. 489–506, Mar. 2009.

[32] T. Loupas, J. T. Powers, and R. W. Gill, "An axial velocity estimator for ultrasound blood flow imaging, based on a full evaluation of the Doppler equation by means of a two-dimensional autocorrelation approach," *IEEE Trans. Ultrason., Ferroelectr. Freq. Control*, vol. 42, no. 4, pp. 672–688, Jul. 1995.

[33] H. Torp, "Clutter rejection filters in color flow imaging: A theoretical approach," *IEEE Trans. Ultrason., Ferroelectr. Freq. Control*, vol. 44, no. 2, pp. 417–424, Mar. 1997.

[34] A. Yu and L. Lovstakken, "Eigen-based clutter filter design for ultrasound color flow imaging: A review," *IEEE Trans. Ultrason. Ferroelectr. Freq. Control*, vol. 57, no. 5, pp. 1096–1111, May 2010.

[35] S. Bjaerum, H. Torp, and K. Kristoffersen, "Clutter filter design for ultrasound color flow imaging," *IEEE Trans. Ultrason. Ferroelectr. Freq. Control*, vol. 49, no. 2, pp. 204–216, Feb. 2002.

[36] K. P. Burnham and D. R. Anderson, "Multimodel inference. Understanding AIC and BIC in model selection," *Sociological Methods Res.*, vol. 33, no. 2, pp. 261–304, 2004.

[37] C. M. Hurvich and C. L. Tsai, "Regression and time series model selection in small samples," *Biometrika*, vol. 76, no. 2, pp. 297–307, 1989.

[38] A. P. Kadi and T. Loupas, "On the performance of regression and step-initialized IIR clutter filters for color Doppler systems in diagnostic medical ultrasound," *IEEE Trans. Ultrason., Ferroelectr. Freq. Control*, vol. 42, no. 5, pp. 927–937, Sep. 1995.

[39] M. I. Gurevich, *Theory of Jets in Ideal Fluids*. New York: Academic, 1965.

[40] O. Bonnefous and P. Pesque, "Time domain formulation of pulse-Doppler ultrasound and blood velocity estimation by cross correlation," *Ultrason. Imag.*, vol. 8, no. 2, pp. 73–85, 1986.

[41] H. Torp and K. Kristoffersen, "Comparison between cross-correlation and auto-correlation technique in color flow imaging," in , *Proc. Ultrason. Symp.*, pp. 1039–1042, 1993.

[42] K. S. Kim, J. S. Hwang, J. S. Jeong, and T. K. Song, "An efficient motion estimation and compensation method for ultrasound synthetic aperture imaging," *Ultrason. Imag.*, vol. 24, no. 2, pp. 81–99, 2002.

[43] L. Xiaoming, H. Torp, and K. Kristoffersen, "An extended autocorrelation method for estimation of blood velocity," *IEEE Trans. Ultrason., Ferroelectr., Freq. Control*, vol. 44, no. 6, pp. 1332–1342, Nov. 1997.

[44] J. Avdal, L. Lovstakken, and H. Torp, "Effects of reverberations and clutter filtering in pulsed Doppler using sparse sequences," *IEEE Trans. Ultrason., Ferroelectr., Freq. Control*, vol. 62, no. 5, pp. 828–838, May 2015.

[45] D. N. Moisseev, C. M. Nguyen, and V. Chandrasekar, "Clutter suppression for staggered PRT waveforms," *J. Atmospheric Oceanic Technol.*, vol. 25, no. 12, pp. 2209–2218, 2008.

[46] J. Y. Cho and E. S. Chornoboy, "Multi-PRI signal processing for the terminal Doppler weather radar. Part I: Clutter filtering," *J. Atmospheric Oceanic Technol.*, vol. 22, no. 5, pp. 575–582, 2005.

[47] S. Fadnes, S. A. Nyrnes, H. Torp, and L. Lovstakken, "Shunt flow evaluation in congenital heart disease based on two-dimensional speckle tracking," *Ultrasound in Med. Biol.*, vol. 40, no. 10, pp. 2379–2391, 2014.

[48] R. Yotti *et al.*, "Noninvasive assessment of ejection intraventricular pressure gradients," *J. Am. Coll. Cardiol.*, vol. 43, no. 9, pp. 1654–1662, 2004.

[49] T. Masuyama *et al.*, "Noninvasive evaluation of aortic regurgitation by continuous-wave Doppler echocardiography," *Circulation*, vol. 73, no. 3, pp. 460–466, 1986.